Original Research

Label-free characterization of collagen fibers in cancerous esophagus tissues using ratiometric nonlinear optical microscopy

Wei-Chung Chen[1,*], Yu-Jen Chen[2,*], Shih-Ting Lin[2], Wei-Han Hung[3], Ming-Che Chan[4], I-Chen Wu[5], Ming-Tsang Wu[6,7], Chie-Tong Kuo[8], Subir Das[9], Fu-Jen Kao[9] and Guan-Yu Zhuo[2,10]

[1]Ph.D. Program in Environmental and Occupational Medicine, Kaohsiung Medical University, Kaohsiung 80708, Taiwan; [2]Integrative Stem Cell Center, China Medical University Hospital, Taichung 40447, Taiwan; [3]Institute of Medical Science and Technology, National Sun Yat-sen University, Kaohsiung 80424, Taiwan; [4]Institute of Photonic System, College of Photonics, National Chiao-Tung University, Tainan 71150, Taiwan; [5]Division of Gastroenterology, Department of Internal Medicine, Kaohsiung Medical University Hospital, Kaohsiung Medical University, Kaohsiung 80708, Taiwan; [6]Department of Public Health, Kaohsiung Medical University, Kaohsiung 80708, Taiwan; [7]Department of Family Medicine, Kaohsiung Medical University Hospital, Kaohsiung 80708, Taiwan; [8]Department of Physics, National Sun Yat-sen University, Kaohsiung 80424, Taiwan; [9]Institute of Biophotonics, National Yang-Ming University, Taipei 11221, Taiwan; [10]Institute of New Drug Development, China Medical University, Taichung 40402, Taiwans
Corresponding author: Guan-Yu Zhuo. Email: zhuo0929@mail.cmu.edu.tw
*These authors contributed equally to this work.

Impact statement

The issue of classifying esophageal cancer at various developmental stages is crucial for determining the optimized treatment protocol for the patients, as well as the prognosis. Precision improvement in staging esophageal cancer keeps seeking quantitative and analytical imaging methods that could augment histopathological techniques. In this work, we used nonlinear optical microscopy for ratiometric analysis on the intrinsic signal of two-photon excited fluorescence (TPEF) and second harmonic generation (SHG) from single collagen fibers only in submucosa of esophageal squamous cell carcinoma (ESCC). The blind tests of TPEF/SHG and forward (F)/backward (B) SHG were demonstrated to compare with the histology conclusion. The discussion of sensitivity and specificity was provided via statistical comparison between the four stages of esophageal cancer. To the best of our knowledge, this is the first study of using these two ratios in combination for staging ESCC.

Abstract

A quantitative analytical method to discriminate among the various types of cancerous esophagus tissue is essential for accurate cancer staging. This paper reports on the use of ratiometric nonlinear optical microscopy to reveal the ratio of two-photon excited fluorescence (TPEF) to second harmonic generation (SHG) and forward to backward (F/B) SHG from single collagen fibers only in submucosa of esophageal squamous cell carcinoma. This makes it possible to accurately differentiate among the four stages of esophageal cancer, providing results that are in good agreement with histopathology. Furthermore, it is confirmed by polarization-dependent SHG that the varied SHG response in esophageal cancer tissues is mainly from the shrinkage in diameter of collagen fibers instead of the collagen triple helixes altered by cancer cells. Based on the results of TPEF/SHG and F/B SHG ratio, they can cooperatively improve the precision of diagnostics on esophageal cancer and could be transferred to other types of cancer diseases with changed collagen fibers.

Keywords: Esophageal cancer, nonlinear optical microscopy, second harmonic generation, two-photon excited florescence, esophageal squamous cell carcinoma, collagen fiber

***Experimental Biology and Medicine* 2020; 245: 1213–1221. DOI: 10.1177/1535370220934039**

Introduction

The incidence of esophageal cancer has doubled worldwide over the past two decades, and esophageal cancer is counted as one of the top 10 causes of cancer death worldwide. In this type of cancer, tumors are aggressive and present as two distinct histologic types: esophageal squamous cell carcinoma (ESCC) and esophageal adenocarcinoma (EADC). Both types are developed from the same epithelial lining of esophagus, but induced by different etiological factors. ESCC arise from the exposure to premalignant risk factors, causing chronic inflammation, and it shows squamous cell features such as keratin pearls and keratinization in well differentiated cells. On the other hand, EADC experience multiple genetic abnormalities accumulation, and it shows the gland tumor features such as tubular or papillary growth.[1] The incidence of ESCC has decreased in western countries over the last 40 years;[2,3] however, it remains the most common type of esophageal cancer in Asia and Sub-Saharan Africa.[4] Early ESCC is usually asymptomatic, which means that more than half of patients are already in advanced stages or have tumors that have metastasized when they are diagnosed, resulting in a five-year survival rate of only 10%. Precise staging of ESCC is crucial in more advanced stages, due to the importance of determining the appropriate treatment modality and defining the prognosis. Recent guidelines suggest neoadjuvant therapy prior to surgery for stage IIb or III esophageal cancer, whereas direct esophagectomy is recommended for stage I and IIa.[5] Nonetheless, researchers continue to debate the use of adjuvant therapy for ESCC, partly due to the toxicity of treatment. Existing results show that conventional hematoxylin and eosin (H&E) staining, fast Fourier transform, and spectroscopic analysis have proven highly effective in differentiating normal tissue from cancerous tissue. However, due to non-representative biopsies, imperfect sample preparation, or the selected region of interests (ROIs), it is often difficult to further subdivide cancerous tissues. Therefore, a more objective method by obtaining the structural/spectroscopic information of single collagen fibers might be a possible route for cancer stage classification. Currently, there are also limitations in the pathological diagnosis of cancer status and in the ability to identify individuals who are susceptible to early recurrence, i.e. patients who require aggressive treatments. Pathologists are therefore in need of new methods to improve the speed and accuracy of esophageal cancer staging.

To assist pathologists, researchers have yet to devise optical imaging techniques with sufficient precision to assist in the diagnosis of esophageal cancer. Thus, cancer detection relies heavily on endoscopic techniques, such as image-enhanced endoscopy.[6,7] A number of recent advances have been shown to facilitate the visualization of tumors; however, precise cancer staging is hampered by insufficient image contrast, physician bias, and the fact that images only reveal the surface of tumors. These limitations have led to the development of advanced optical imaging tools to augment histopathological techniques in cancer research, including confocal microscopy and two-photon excited fluorescence (TPEF)/second harmonic generation (SHG) microscopy.[8,9] Methods which employ these tools show considerable promise in elucidating the microstructure of bio-tissues and in monitoring the structural changes associated with tumor progression. Nevertheless, lots of imaging schemes based on confocal microscopy usually require fluorescent labeling to enhance image contrast, which may undermine the precision in diagnostics, and disturb the way a biological event functions. Alternatively, TPEF/SHG microscopy facilitates label-free and noninvasive imaging and has proven successful in the early diagnosis of ovarian cancer, breast cancer, and gastric cancer.[10–13]

TPEF microscopy uses a near-infrared femtosecond laser to produce fluorescent photons. The sources of TPEF in a cancerous esophagus are dominated by collagen, elastin, and other enzymatic proteins associated with the metabolic activities of cancer cells, such as flavin adenine dinucleotide (FAD) and nicotinamide adenine dinucleotide (NADH). Using the same laser source, SHG microscopy can detect collagenous tissues, due to well-arranged fibrils constituted by a triple-helix of collagen molecules. One dominant phenomenon showing the proportion of collagen fibers decreases as submucosa is infiltrated by cancer cells and can be characterized by the SHG contrast.[14] Moreover, the intensity ratio between TPEF and SHG provides information related to the composition and structure of collagen fibers, which can be used to verify whether the tissue is cancerous or normal.[15]

The content, structure, and distribution of collagen and elastic fibers have been verified. Furthermore, the nuclear size of normal and cancerous esophagus in submucosa layer is also discussed.[15–17] Because collagen fibers are the source of TPEF and SHG, simultaneous two-channel imaging based on the two signals allows ratiometric analysis on single collagen fibers.[13,18,19] The intensity ratio between them will be used as one parameter for cancer staging. On the other hand, SHG is a coherent process describing the constructive build-up of nonlinear light scattering in forward and backward direction following different phase-matching conditions. Because the phase-matching condition strictly depends on the refractive index and size (diameter or thickness) of single collagen fibers,[20,21] the ratio of forward to backward (F/B) SHG analyzing from the obtained images will be served as an additional parameter for evaluating cancer stage.

Materials and methods

Preparation of tissue slides

The ESCC tissue specimens were provided from 13 esophageal-cancer patients involved in the experiments and their pathological characteristics are summarized in Table 1. Patients were enrolled in this study based on the following criteria: (i) those older than 20 years; (ii) pathologically confirmed as ESCC initially; (iii) who had sufficiently archived tissue blocks; and (iv) who had lived at least more than one month after surgical resection. The exclusion criteria were: patients (i) who had multiple

Table 1. Clinical characteristics of 13 esophageal-cancer patients.

Patient	Gender	Age	Cancer classification	Stages
1	Male	64	Esophageal squamous cell carcinoma	I
2	Male	61	Esophageal squamous cell carcinoma	I
3	Male	66	Esophageal sarcomatoid carcinoma	I
4	Male	44	Esophageal squamous cell carcinoma	IIA
5	Male	68	Esophageal squamous cell carcinoma	IIA
6	Male	47	Esophageal squamous cell carcinoma	IIA
7	Male	71	Esophageal squamous cell carcinoma	IIB
8	Male	60	Esophageal squamous cell carcinoma	IIB
9	Male	51	Esophageal carcinoid	IIB
10	Male	39	Esophageal sarcomatoid carcinoma	III
11	Male	50	Esophageal squamous cell carcinoma	III
12	Male	35	Esophageal squamous cell carcinoma	IV
13	Male	42	Esophageal squamous cell carcinoma	IV

primary cancers; (ii) who had insufficient archived tissue blocks.

All tissue was fixed in 4% buffered neutral formalin for 24 h and then dehydrated using a gradient ethanol bath, followed by xylene clearance and embedding in paraffin. The tissue blocks were sectioned into slices with an average thickness of 5 μm, and then attached to charged glass slides prior to incubation at 37°C overnight. The tissue slides were deparaffinized via xylene clearance three times, and were mounted with Canadian balsam mounting medium. Finally, the slides were left air-drying overnight.

Thirteen ESCC patients who attended the previous studies (KMUHIRB-GENE-20110004 and KMUHIRB-G(I)-20170017) had enrolled in this study. All the patients in both studies had been acknowledged that their tissue would be used for other esophageal cancer studies when signing the informed consent. This study protocol was approved by the institutional review board of Kaohsiung Medical University Hospital (KMUH). In this IRB application, we requested to exempt the informed consent because all enrolled patients had expired before this study.

Nonlinear optical cancer imaging

In our experiment, we have combined a Ti:sapphire mode-locked laser (Mira 900, Coherent) that generates central wavelength of 810 nm, pulse repetition rate of 76 MHz, and pulse width approximately of 200 fs with our microscope system (IX 71, Olympus). The average laser power was maintained at 20 mW, which was deemed sufficient to produce SHG and TPEF while preventing photodamage under continuous illumination. The wavelength of SHG from collagen fibers was 405 nm, whereas the TPEF from collagen fibers ranged from 450 to 570 nm.[9,15,22] All of the images were obtained using a laser scanning unit (Fluoview 300, Olympus), a pair of objective lenses for laser focusing and the collection of photons (UPlanSApo 20×/0.75, Olympus), and two photomultiplier tubes for the detection of forward/backward SHG and backward TPEF (R3896, Hamamatsu). In backward imaging mode, SHG and TPEF were split using a dichroic beamsplitter (FF435-Di01, Semrock), and filtered from the intense excitation laser background using a bandpass filter (FF01-405/10, Semrock) and a colored glass (BG39, Schott), respectively. In F/B-SHG imaging, the filter used for F-SHG was the same as B-SHG. Additionally, we used the polarization-dependent SHG of collagen fibers to derive the ratio of tensor elements of second-order susceptibility $\chi^{(2)}$, which reflects the molecular structure of collagen triple helix. This measurement was conducted using a rotary (rotation with 10° increment from 0° to 180°) half-wave plate (AHWP05M-980, Thorlabs) and a quarter-wave plate for polarization ellipticity compensation (AQWP05M-980, Thorlabs) inserted in the beam path for imaging.[5] It is noted that to have a precise estimation on cancer stage, a pair of same PMT are used with the same gain level for image acquisition. Besides, a 50/50 beamsplitter (BSW10R, Thorlabs) is used to correct the detection efficiency for two PMTs prior to ratiometric analysis. Furthermore, throughout the measurements, it is required to fix the axial position of the condenser lens in order to preserve the same laser-focusing and photon-collection schemes, guaranteeing a meaningful and accurate estimation. The acquired images were mainly processed and analyzed with ImageJ and Matlab software.

Statistical analysis

Before statistics, the paired images for ratiometric analysis are processed with noise removal. The noise level is defined as the area in the absence of esophagus tissues. All the images used for analysis should subtract the same value to keep the analyzing condition consistent. In statistics, the ratio in each experiment is represented as mean ± standard deviation, and the one-way ANOVA test is used to detect differences within groups followed by Tukey's multiple comparison test. In TPEF/SHG imaging, the image patterns taken from the two modalities are different since other substances can exhibit fluorescence except collagen fibers. Thus, direct division from the paired images will produce markable variations. To avoid this problem, the fiber region segmented is followed by the following three rules: (i) The selected ROI should have both SHG (color in green) and TPEF (color in red) signals, which exhibits yellow color in the merged image; (ii) The region at which two collagen fibers are overlapped or staggered cannot be used since only the ROI containing single collagen fibers is allowable; (iii) 200 ROIs, each encircled by the area with 5 × 5 pixels, only containing single collagen fibers for each cancer stage are selected for statistical analysis. In F/B SHG imaging, it is free from the first rule as the image patterns are nearly identical with the paired images, while the other two rules should be kept for a precise estimation on cancer stage. Note that the TPEF/SHG ratio was

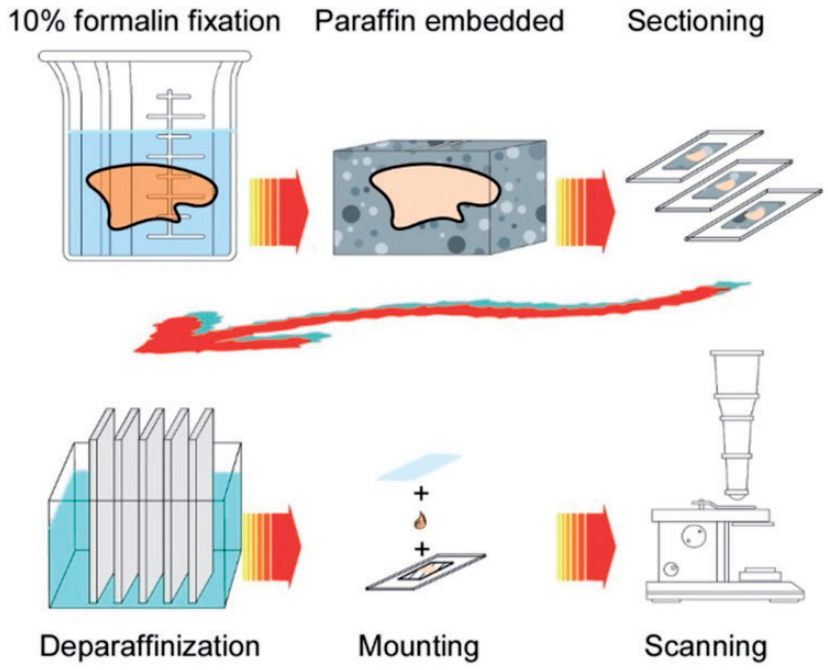

Figure 1. Flowchart illustrating the preparation of ESCC tissue samples. The tissues were fixed in 10% formalin to stabilize the tissue structure before being embedded in paraffin and sectioned into slices with a thickness of 5 μm for mounting on glass slides. Following removal of the paraffin and rehydration using an alcohol-water mixture, the tissues were sent for laser scanning imaging. (A color version of this figure is available in the online journal.)

calculated by dividing the average TPEF and SHG intensities over the 5×5-pixels ROI, while the B/F SHG ratio was also calculated using the same approach.

Results and discussion

Visualizing the morphological structure of cancerous esophagus tissue

Figure 2 presents the cancerous tissues in four different stages as imaged using SHG and TPEF. In Figure 2(a), a large field of view in cancerous tissues clearly shows that the collagen fibers (fibrous-like in yellow to green) used for analysis are located in submucosa (encircled by white-dashed lines). Only the area selected is intended to reduce bias of the results and the sampling error issues inherent to histopathology analysis such as non-representative biopsies imperfect sample preparation or the selected region of interests. The content of collagen fibers decreases with the progression of cancer can be found from the statistical analysis on multiple SHG images of Stages-I to IV, as shown in Figure 2(b) to (e). This phenomenon occurs when the cancer cells gradually proliferate into the submucosa and the extracellular collagen is degraded. The Stage I morphology presented in Figure 2(b) shows an abundance of randomly organized and crimped collagen fibers. Stage I is characterized by widely distributed large fibers (1.86 ± 0.33 μm). Stage II (Figure 2(c)) is characterized by a bit thinner and sparser collagen fibers (1.35 ± 0.26 μm). In Stages III and IV (Figure 2(d) and (e)), it is obvious that the tissues lose lots of collagen fibers, which are comparatively much thinner, sparser, and fragmented (1.19 ± 0.24 and 1.01 ± 0.17 μm are their collagen fiber diameter, respectively). Note that the analysis of randomness has been performed by the ellipse fit to fast Fourier transform (FFT) spectrum of the image. If the ratio of major to minor axis of the ellipse is close to 1, the collagen fiber orientation is defined as high randomness.[23] On the other hand, the estimation of collagen fiber diameter is measured with various straight lines via ImageJ software across single collagen fibers. The statistical results for each cancer stage are shown in Figure 2(f).

Because tissues with malignant tumors often lead to abnormal collagen assembly in contrast to normal tissues, the analysis of collagen architecture by SHG has become a promising approach for diagnosing cancers.[24,25] Recently, the ratio of SHG pixels to total pixels in an image can be used in the staging of cancerous tissues, as demonstrated in studies of gastric carcinoma.[26] However, assessment using this method is not reliable in our case because the diagnostic precision is easily affected by the sampling error issues as mentioned above. On the other hand, although the basement membrane and basal cell layer are two diagnostic features that have been used to distinguish normal esophagus from carcinoma *in situ*,[16] it is challenging to stage the cancer based on H&E-stained histological image because the two features are either hardly noticeable or highly destroyed in advanced tumor stages. Without obvious and regular cancer cells occupied in the examined tissues, most of the areas contain connective tissues, as shown in Figure 2(g) and (h). Therefore, to get extra valuable information to help cancer staging, it needs the structural/spectroscopic information of single collagen fibers to support an objective, quantitative, and precise assessment, which are described in the following sections.

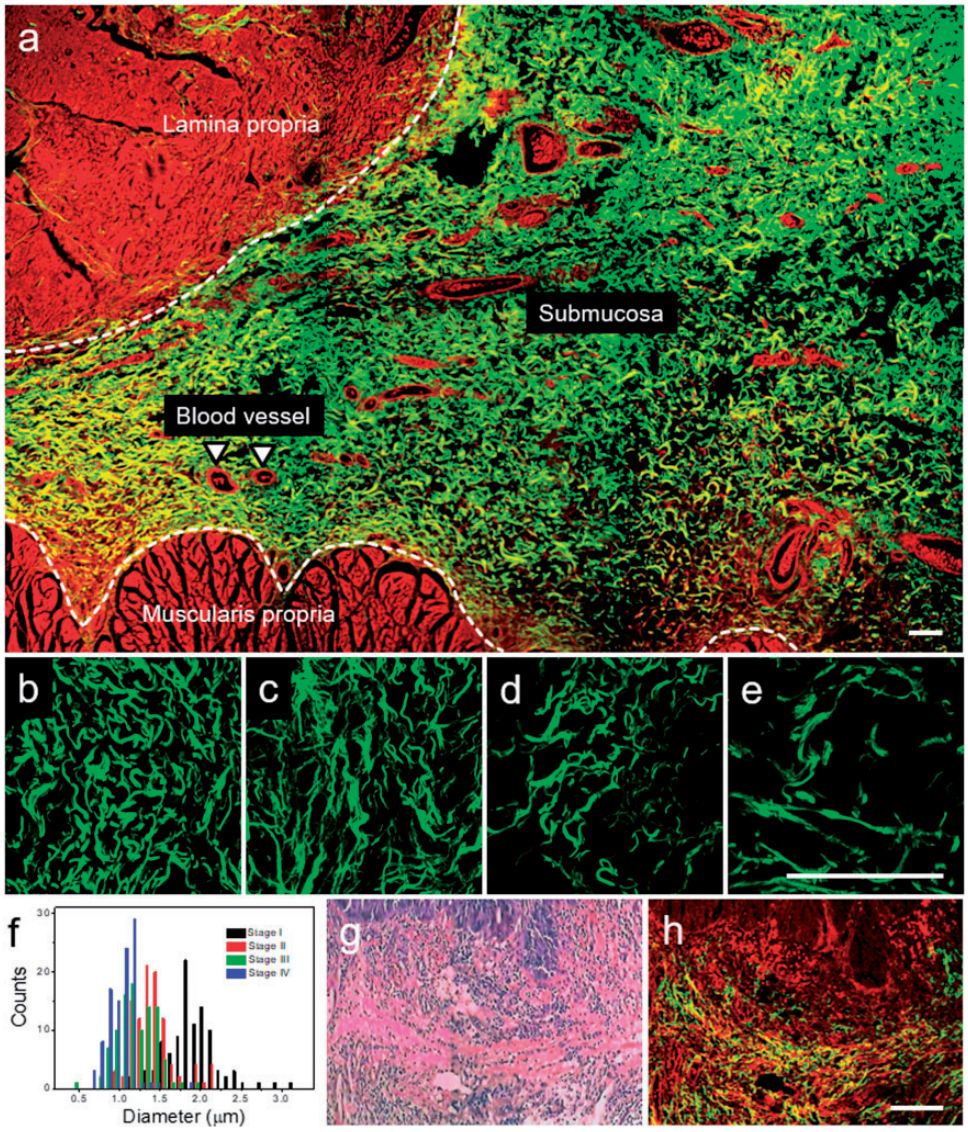

Figure 2. (a) A large-field-of-view image showing the surrounding environment and macrostructure of submucosa in cancerous tissues, where green is SHG, red is TPEF, and yellow is the merge of SHG and TPEF. Note that different from other figures shown in this manuscript, it is imaged with a large field of view using a low-magnification objective lens (UPlanSApo 10×/0.4, Olympus) along with mosaic imaging approach to characterize the morphological structure of submucosa in cancerous tissues (Stage I). (b)–(e) are the SHG images that present the morphological structure, orientation, and density of collagen fibers in submucosa corresponding to Stages I to IV, respectively. (f) is the histogram of the diameter of collagen fibers for each stage ($n = 100$). (g) and (h) are the H&E-stained histological image and nonlinear optical image taken at the same position (Stage IV). Scale bar: 100 μm. (A color version of this figure is available in the online journal.)

Cancer staging using the intensity ratio of TPEF/SHG

Nonlinear optical microscopy has been extensively used for the diagnosis of cancer diseases based on specific estimating parameters, which are tabulated in Table 2 as an overview on the existing applications. Among them, the intensity ratio of TPEF/SHG has been used to differentiate between cancerous and normal tissues;[15,17,27,28] however, to our knowledge, this approach has not previously been used for the staging of ESCC. Here we investigated the single collagen fibers in submucosa of cancerous tissues and counted the intensities of TPEF and SHG for ratiometric analysis. One of the representative image pairs is shown in Figure 3(a) to (c), and the statistic results of TPEF/SHG ratio at each stage are shown in Figure 3(d). The results from Stages I to IV are in sequence of 1.43 ± 0.18, 0.94 ± 0.23, 0.52 ± 0.10, and 0.30 ± 0.08, respectively. These results are statistically different when compared to each other group ($P < 0.001$). Based on the result that TPEF/SHG ratio is inversely proportional to the stage number, thereby, the decreasing percentage of TPEF is higher than that of SHG. For the more pronounced decrease in TPEF, it can be explained by the fact that the collagen fibers are decomposed with a reduction in the concentration of collagen cross-links, which is influenced by the enzyme secretion of cancer cells.[29] It is similar to the result of Liu *et al.* which focused on collagen fibers only. However, our measured values are larger than those of Liu *et al.*[15] (~0.36 in normal collagen and ~0.20 in cancerous collagen in submucosa), which refers to the differences in PMT sensitivity, the

Table 2. Some representative examples of using nonlinear optical microscopy for the diagnosis of cancer diseases.

Cancer type	Source	How to identify normal and cancerous tissues	Refs.
Breast cancer	1 breast cancer cell line	Combination of TPEF and lipid fraction imaging	30
Breast cancer	30 tumor and 30 normal tissues	Cell nuclear-cytoplasmic ratio	31
Breast cancer	12 tumor and 30 normal tissues	Microstructure	32
Colorectal cancer	5 normal, 5TMMSC, and 5 TMSSC tissues	Collagen content and orientation	33
Colorectal cancer	7 tumor and 7 distant normal tissues (Paired)	TPEF/SHG ratio	27
Gastric cancer	12 tumor and 12 normal tissues	Average SHG intensity per pixel	34
Gastric cancer	18 tumor tissues	Nuclear size and collagen content	26
Gastrointestinal neuroendocrine tumors	20 tumor tissues	Nuclear-cytoplasmic ration and collagen content	35
Esophageal cancer	4 tumor tissues	Collagen fiber content and orientation	9
Esophageal cancer; rabbit	20 rabbits, 97.67% of them generated tumor	TPEF and SHG micro-anatomical information	36
Esophageal cancer	9 tumor and 9 normal tissues (Paired)	Collagen distance and TPEF/SHG ratio	28
Esophageal cancer	10 tumor and 10 normal tissue (Paired)	Collagen orientation and TPEF/SHG ratio	17
Esophageal cancer	20 tumor and 20 distant normal (Paired)	TPEF/SHG ratio	15
Lung cancer	LSL-K-Ras G12D mutant mice	Distinct morphologies and fluorescence emission properties	37
Lung cancer	33 tumor, 13 desmoplastic edge, and 6 normal tissues	Collagen fiber content and elastin fiber content	38
Melanoma	5 melanoma, 5 dysplastic nevi, and 5 common nevi	MMI index from MPM image pixel intensity, collagen fiber across epidermal-dermal junction, and melanocytic dendrites density	39
Head and Neck cancer	12 tumor tissues	Fully convolutional neural networks training	40
Rectal cancer	32 tumor tissues	Collagen density and orientation	41

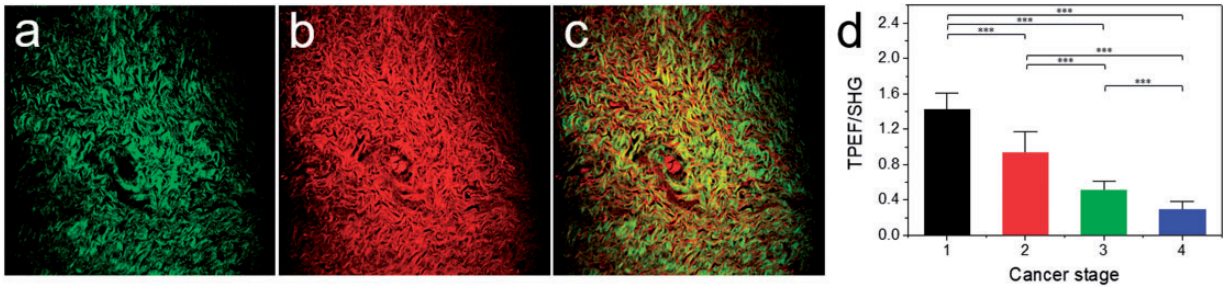

Figure 3. (a)–(c) are the representative images (Stage I) of collagen fibers in submucosa obtained from SHG, TPEF, and merge of the two. Image size: $600 \times 600\ \mu m^2$. (d) is the statistic results for TPEF/SHG ratio on the four stages of cancerous tissues. The standard deviation is represented by an error bar. *** indicates $P < 0.001$. (A color version of this figure is available in the online journal.)

transmittance and/or reflectance of used filters and dichroic mirrors, and sample preparation processes (e.g. alcohol may somewhat denature collagen and then affects the SHG intensity; a little TPEF intensity from fixation is added on natural fluorescence emanating from collagen fibers). As a comparison, reversed results were reported in Chen *et al.* [17] and Zhuo *et al.*, probably because they both took total SHG and TPEF into account, rather than focusing on collagen fibers only as in Liu *et al.*[15] and our work. Although the conditions used in each experiment are different, the results can all conform to their specific assumptions and are well confirmed experimentally. Consequently, this method might be applied to early diagnosis and/or staging of cancer if the tissue has intrinsic substances allowing for wavelength conversion through nonlinear optical processes.

Cancer staging using the intensity ratio of forward to backward SHG

Followed by the above measurements, the forward detection of SHG can be easily interfaced with the microscope to demonstrate simultaneous two-channel imaging of forward (F) and backward (B) SHG. It has been proven that due to different phase-matching constraints (i.e. different coherence lengths), F-SHG is stronger in well-formed thick tissues, while B-SHG is dominated in thin slice samples or small and segmented features in tissues. Such difference has been translated into a molecular contrast showing the information of order of the inter-fibril structure, density of bundles, fibril thickness or diameter, and the capability of selective imaging.[20,21,42,43] According to the above issues on local collagen structure and tissue optical properties, we used the ratio of F/B SHG to confirm the feasibility of cancer staging. Figure 4(a) to (c) presents one representative image pair for the analysis, and Figure 4(d) shows the statistic results of F/B SHG ratio for each stage, of which the values from Stages I to IV are in sequence of 9.46 ± 1.23, 8.30 ± 1.05, 5.55 ± 0.82, and 4.26 ± 0.69, respectively. These results are statistically different when compared to each other group ($P < 0.001$). Similar to the trend of TPEF/SHG, the F/B SHG ratio is moving toward a lower value

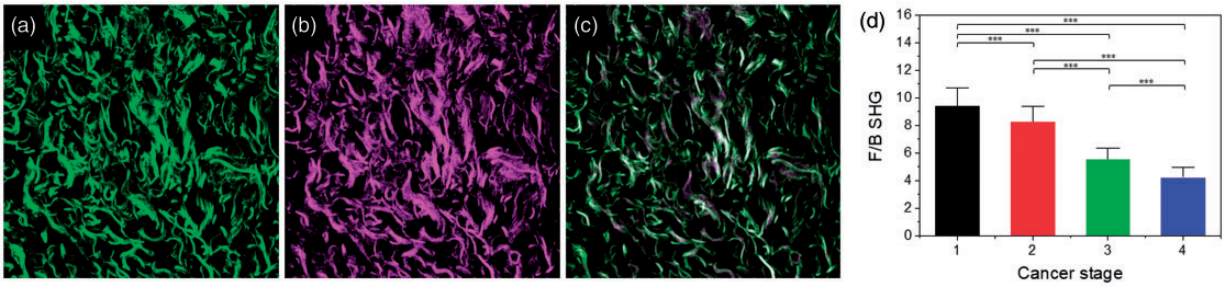

Figure 4. (a)–(c) are the representative images (Stage I) of collagen fibers in submucosa obtained from F-SHG, B-SHG, and merge of the two. Image size: 300 × 300 μm^2. (d) is the statistic results for F/B SHG ratio on the four stages of cancerous tissues. The standard deviation is represented by an error bar. *** indicates $P < 0.001$. (A color version of this figure is available in the online journal.)

as the stage number increases, which indicates that the diameter of collagen fibers is shrunken when cancer cells infiltrate into submucosa. This result complies well with the calculation of collagen fiber diameter in 'Visualizing the morphological structure of cancerous esophagus tissue' section. According to Figure 4(d), it provides a precise estimation of cancer stage, as an effective aid to support the result of TPEF/SHG, which is inaccessible by current endoscopy techniques. Therefore, the optical signature of F/B SHG ratio could be validated in cancer research for analyzing the changed collagen fibers.

Studying the molecular structure of collagen by polarization-dependent SHG

Specific symptom resulting in the structure change of collagen is either at molecular scale or macromolecular scale. For example, osteogenesis imperfecta (OI) is based on the mutations in the collagen triple helix.[44] Thus, to understand the reason behind SHG variation, it is required to both perform the measurements at molecular and macromolecular scale. Then, through comparative analysis of specific experiments, the dominant factor can be found for staging esophageal cancer.

SHG is a second-order nonlinear optical process, wherein the strength of induced nonlinear polarization is related to the direction of laser polarization with respect to the molecular dipole orientation in bio-tissues. SHG radiation can be formulated using a structural tensor $\chi^{(2)}$, while the corresponding SHG intensity is described by multiplying $\chi^{(2)}$ with the imposed electric field. An example of this is presented in literature.[45–49] By manipulating the electric field (i.e. the polarization state), the dependence of SHG intensity on variations in the polarization states appears in each pixel in the images. The structural information, such as intrinsic optical nonlinearities, three-dimensional orientation of SHG-active molecules, molecular packing symmetry, and the helical pitch angle of SHG-active molecules, can all be obtained via $\chi^{(2)}$ tensor analysis. It has been evidenced that χ_{33}/χ_{31} is a key factor to differentiate different kinds of SHG-active molecules because it determines the degree of folding of helical molecules as well as the degree of organization of proteins in tissues.[50,51] In addition, this value was found to be subject to the type and age of tissue as well as mechanical tension (i.e. values were closely related to the molecular structure of collagen fibrils).[51] Therefore, it is very likely that χ_{33}/χ_{31} values pose great possibilities to be a parameter to quantify the architecture of collagen molecules.

For $\chi^{(2)}$ analysis, it needs a molecular model providing the spatial definition of collagen molecules.[49] Based on the assumption of cylindrical symmetry and $\chi^{(2)}$ tensor transformation from molecular frame to laboratory frame, the SHG intensity is written as

$$I^{2\omega} \sim \left[\left(\frac{\chi_{15}}{\chi_{31}} \sin 2(\theta - \theta_0) \right)^2 + \left(\sin^2(\theta - \theta_0) + \frac{\chi_{33}}{\chi_{31}} \cos^2(\theta - \theta_0) \right)^2 \right] \quad (1)$$

where θ and θ_0 are the angle of laser polarization direction and planner orientation of collagen molecules, respectively. Through data fitting to the SHG polarization dependencies at each image pixel by equation (1), θ_0, χ_{33}/χ_{31}, and χ_{15}/χ_{31} are determined. Figure 5(a) to (d) illustrates the results of the distribution of χ_{33}/χ_{31} for each stage ($n = 25$) in terms of color-coded images extracted by polarization-dependent SHG. For the shape of histograms in Figure 5(e), these distributions are kind of similar, but the P-value of Stages-III to II and Stages-III to IV is less than 0.05. Except the two combinations, the measured P-values are all larger than 0.05, and the shift of peaks does not show any relationship between the cancer stages. Combined with the results at the macromolecular scale (i.e. TPEF/SHG and F/B SHG ratio measured on collagen fibers), it is concluded that the $\chi^{(2)}$ ratio cannot be used for cancer staging and the SHG variation is mainly from the macromolecular structure of collagen fibers rather than the molecular structure of collagen triple helix.

Conclusions

In this study, we employed nonlinear optical microscopy to perform detailed and quantitative analysis of various types of esophageal cancerous tissues from ESCC patients. The characterization of morphological structure of submucosa and structural information of single collagen fibers for cancer staging was demonstrated. Since the existing optical microscopy approaches are difficult to stage cancer precisely, we performed comparative analyses among four different stages of cancerous tissues and the relative changes in the ratio of TPEF/SHG and F/B SHG can be used for a

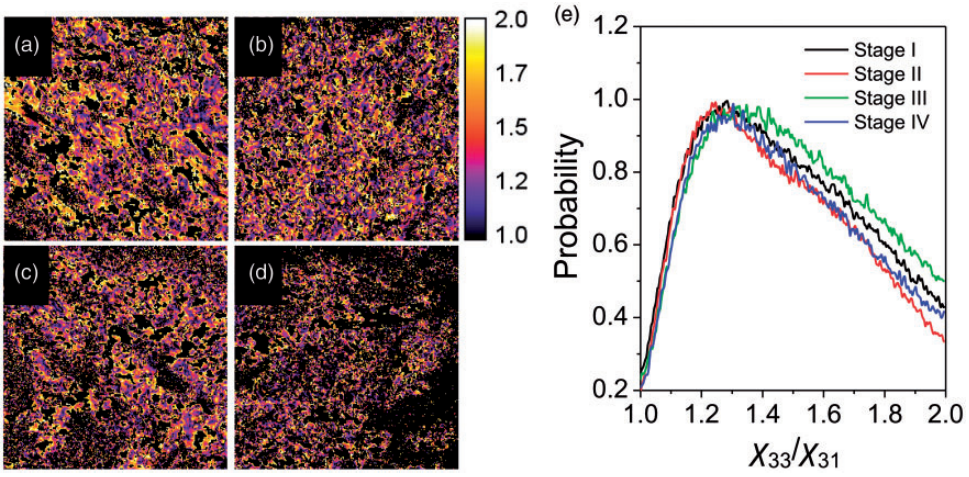

Figure 5. (a)–(d) are the results of χ_{33}/χ_{31} from Stages I to IV, respectively, which are registered by fire color scale. The color bar is shown beside (b). (e) shows the corresponding distributions are nearly identical, indicating that the collagen structure is not greatly changed during tumor progression at the molecular scale. Image size: $300 \times 300\ \mu m^2$. (A color version of this figure is available in the online journal.)

reliable cancer diagnosis. Meanwhile, the sampling error issues such as non-representative biopsies, imperfect sample preparation, or the selected region of interests can be suppressed by confining the investigation only at submucosa. Based on the experimental results, our approach confirmed the potentiality of nonlinear optical microscopy and could draw diagnostic impact on histological evaluation of cancer diseases. In the future, this imaging method could be further tested on nonlinear optical endoscopy to monitor tumor progression with an *in vivo*, label-free, and noninvasive imaging.

Authors' contributions: WC, YJ, ST, WH, and GY implemented the experiments and analyzed the results. WC, YJ and GY drafted the manuscript. IC contributed to sample preparation. IC and FJ comment on the idea. MT and CT contributed to funding support. YJ, MC, SD, FJ, and GY discussed the results and reviewed the manuscript. GY perceived the idea, supervised the project, and finalized the manuscript.

ACKNOWLEDGEMENTS

The authors thank the CMU 2-photon imaging core at Integrative Stem Cell Center, China Medical University Hospital, Taiwan for collecting TPEF and SHG images and all participants in this study. This work also acknowledged the Higher Education Sprout Project of the National Chiao Tung University and Ministry of Education (MOE), Taiwan.

DECLARATION OF CONFLICTING INTERESTS

The author(s) declared no potential conflicts of interest with respect to the research, authorship, and/or publication of this article.

FUNDING

This work was funded by Ministry of Science and Technology, Taiwan, 108–2112-M-039–001 and NSYSU-KMU JOINT RESEARCH PROJECT, NSYSUKMU 107-I002.

ORCID IDS

Yu-Jen Chen https://orcid.org/0000-0003-2925-6985
Guan-Yu Zhuo https://orcid.org/0000-0002-9813-2989

REFERENCES

1. Jain S, Dhingra S. Pathology of esophageal cancer and Barrett's esophagus. *Ann Cardiothorac Surg* 2017;**6**:99–109
2. Cook MB, Chow WH, Devesa SS. Oesophageal cancer incidence in the United States by race, sex, and histologic type, 1977–2005. *Br J Cancer* 2009;**101**:855–9
3. Steevens J, Botterweck AA, Dirx MJ, van den Brandt PA, Schouten LJ. Trends in incidence of oesophageal and stomach cancer subtypes in Europe. *Eur J Gastroenterol Hepatol* 2010;**22**:669–78
4. Gupta B, Kumar N. Worldwide incidence, mortality and time trends for cancer of the oesophagus. *Eur J Cancer Prev* 2017;**26**:107–18
5. Ajani JA, D'Amico TA, Bentrem DJ, Chao J, Corvera C, Das P, Denlinger CS, Enzinger PC, Fanta P, Farjah F, Gerdes H, Gibson M, Glasgow RE, Hayman JA, Hochwald S, Hofstetter WL, Ilson DH, Jaroszewski D, Johung KL, Keswani RN, Kleinberg LR, Leong S, Ly QP, Matkowskyj KA, McNamara M, Mulcahy MF, Paluri RK, Park H, Perry KA, Pimiento J, Poultsides GA, Roses R, Strong VE, Wiesner G, Willett CG, Wright CD, McMillian NR, Pluchino LA. Esophageal and Esophagogastric Junction Cancers, Version 2.2019, NCCN Clinical Practice Guidelines in Oncology. *J Natl Compr Canc Netw* 2019;**17**:855–83
6. Singh R, Owen V, Shonde A, Kaye P, Hawkey C, Ragunath K. White light endoscopy, narrow band imaging and chromoendoscopy with magnification in diagnosing colorectal neoplasia. *World J Gastrointest Endosc* 2009;**1**:45–50
7. Chung CS, Lo WC, Lee YC, Wu MS, Wang HP, Liao LJ. Image-enhanced endoscopy for detection of second primary neoplasm in patients with esophageal and head and neck cancer: a systematic review and meta-analysis. *Head Neck* 2016;**38**:E2343–9
8. Kara MA, DaCosta RS, Streutker CJ, Marcon NE, Bergman J, Wilson BC. Characterization of tissue autofluorescence in Barrett's esophagus by confocal fluorescence microscopy. *Dis Esophagus* 2007;**20**:141–50
9. Xu J, Kang D, Zeng Y, Zhuo S, Zhu X, Jiang L, Chen J, Lin J. Multiphoton microscopy for label-free identification of intramural metastasis in human esophageal squamous cell carcinoma. *Biomed Opt Exp* 2017;**8**:3360–8
10. Nadiarnykh O, LaComb RB, Brewer MA, Campagnola PJ. Alterations of the extracellular matrix in ovarian cancer studied by second harmonic generation imaging microscopy. *BMC Cancer* 2010;**10**:94

11. Bredfeldt JS, Liu Y, Pehlke CA, Conklin MW, Szulczewski JM, Inman DR, Keely PJ, Nowak RD, Mackie TR, Eliceiri KW. Computational segmentation of collagen fibers from second-harmonic generation images of breast cancer. *J Biomed Opt* 2014;**19**:016007
12. Yan J, Chen G, Chen J, Liu N, Zhuo S, Yu H, Ying M. A pilot study of using multiphoton microscopy to diagnose gastric cancer. *Surg Endosc* 2011;**25**:1425–30
13. Perry SW, Burke RM, Brown EB. Two-photon and second harmonic microscopy in clinical and translational cancer research. *Ann Biomed Eng* 2012;**40**:277–91
14. Chen J, Wong S, Nathanson MH, Jain D. Evaluation of barrett esophagus by multiphoton microscopy. *Arch Pathol Lab Med* 2014;**138**:204–12
15. Liu NR, Chen GN, Wu SS, Chen R. Distinguishing human normal or cancerous esophagus tissue ex vivo using multiphoton microscopy. *J Opt* 2014;**16**:025301
16. Xu J, Kang D, Xu M, Zhuo S, Zhu X, Chen J. Multiphoton microscopic imaging of esophagus during the early phase of tumor progression. *Scanning* 2013;**35**:387–91
17. Chen WS, Wang Y, Liu NR, Zhang JX, Chen R. Multiphoton microscopic imaging of human normal and cancerous oesophagus tissue. *J Microsc* 2014;**253**:79–82
18. Jiang X, Zhong J, Liu Y, Yu H, Zhuo S, Chen J. Two-photon fluorescence and second-harmonic generation imaging of collagen in human tissue based on multiphoton microscopy. *Scanning* 2011;**33**:53–6
19. Sun W, Chang S, Tai DCS, Tan N, Xiao G, Tang H, Yu H. Nonlinear optical microscopy: use of second harmonic generation and two-photon microscopy for automated quantitative liver fibrosis studies. *J Biomed Opt* 2008;**13**:064010
20. Lacomb R, Nadiarnykh O, Townsend SS, Campagnola PJ. Phase matching considerations in second harmonic generation from tissues: effects on emission directionality, conversion efficiency and observed morphology. *Opt Commun* 2008;**281**:1823–32
21. Chu S-W, Tai S-P, Chan M-C, Sun C-K, Hsiao IC, Lin C-H, Chen Y-C, Lin B-L. Thickness dependence of optical second harmonic generation in collagen fibrils. *Opt Exp* 2007;**15**:12005–10
22. Zoumi A, Yeh A, Tromberg BJ. Imaging cells and extracellular matrix in vivo by using second-harmonic generation and two-photon excited fluorescence. *Proc Natl Acad Sci U S A* 2002;**99**:11014–9
23. Wu S, Li H, Yang H, Zhang X, Li Z, Xu S. Quantitative analysis on collagen morphology in aging skin based on multiphoton microscopy. *J Biomed Opt* 2011;**16**:040502
24. Keikhosravi A, Bredfeldt JS, Sagar AK, Eliceiri KW. Chapter 28 – second-harmonic generation imaging of cancer. In: Waters JC, Wittman T (eds) *Methods in cell biology.* Cambridge, MA: Academic Press, 2014, pp. 531–46
25. Chen X, Nadiarynkh O, Plotnikov S, Campagnola PJ. Second harmonic generation microscopy for quantitative analysis of collagen fibrillar structure. *Nat Protoc* 2012;**7**:654–69
26. He K, Zhao L, Huang X, Ding Y, Liu L, Wang X, Wang M, Zhang Y, Fan Z. Label-free imaging for T staging of gastric carcinoma by multiphoton microscopy. *Lasers Med Sci* 2018;**33**:871–82
27. Li LH, Chen ZF, Wang XF, Zhuo SM, Li HS, Jiang WZ, Guan GX, Chen JX. Multiphoton microscopy for tumor regression grading after neoadjuvant treatment for colorectal carcinoma. *World J Gastroenterol* 2015;**21**:4210–5
28. Zhuo S, Chen J, Xie S, Hong Z, Jiang X. Extracting diagnostic stromal organization features based on intrinsic two-photon excited fluorescence and second-harmonic generation signals. *J Biomed Opt* 2009;**14**:020503
29. Pavlova I, Sokolov K, Drezek R, Malpica A, Follen M, Richards-Kortum R. Microanatomical and biochemical origins of normal and precancerous cervical autofluorescence using laser-scanning fluorescence confocal microscopy. *Photochem Photobiol* 2003;**77**:550–5
30. Hou J, Williams J, Botvinick EL, Potma EO, Tromberg BJ. Visualization of breast cancer metabolism using multimodal nonlinear optical microscopy of cellular lipids and redox state. *Cancer Res* 2018;**78**:2503–12
31. Wu X, Chen G, Qiu J, Lu J, Zhu W, Chen J, Zhuo S, Yan J. Visualization of basement membranes in normal breast and breast cancer tissues using multiphoton microscopy. *Oncol Lett* 2016;**11**:3785–9
32. Wu Y, Lin Y, Lian Y, Lin P, Wang S, Fu F, Wang C, Chen J. Identifying two common types of breast benign diseases based on multiphoton microscopy. *Scanning* 2018;**2018**:3697063
33. Qiu J, Jiang W, Yang Y, Feng C, Chen Z, Guan G, Zhuo S, Chen J. Monitoring changes of tumor microenvironment in colorectal submucosa using multiphoton microscopy. *Scanning* 2015;**37**:17–22
34. Li L, Kang D, Huang Z, Zhan Z, Feng C, Zhou Y, Tu H, Zhuo S, Chen J. Multimodal multiphoton imaging for label-free monitoring of early gastric cancer. *BMC Cancer* 2019;**19**:295
35. Li L, Jiang L, Chen Z, Kang D, Yang Z, Liu X, Jiang W, Zhuo S, Guan G, Zhou Y, Chen J. Nonlinear optical microscopy for label-free detection of gastrointestinal neuroendocrine tumors. *Lasers Med Sci* 2016;**31**:1285–91
36. Ma L, Huang X, Wang X, Zhang Y, Liu L, Sheng Y, Fan Z. Study on the diagnosis of rabbit VX2 esophageal cancer and stent-therapy efficacy based on multiphoton microscopy. *Scanning* 2015;**37**:152–7
37. Pavlova I, Hume KR, Yazinski SA, Peters RM, Weiss RS, Webb WW. Multiphoton microscopy as a diagnostic imaging modality for lung cancer. *Proc SPIE Int Soc Opt Eng* 2010;**7569**:756918
38. Xu X, Cheng J, Thrall MJ, Liu Z, Wang X, Wong ST. Multimodal nonlinear optical imaging for label-free differentiation of lung cancerous lesions from normal and desmoplastic tissues. *Biomed Opt Exp* 2013;**4**:2855–68
39. Balu M, Kelly KM, Zachary CB, Harris RM, Krasieva TB, Konig K, Durkin AJ, Tromberg BJ. Distinguishing between benign and malignant melanocytic nevi by in vivo multiphoton microscopy. *Cancer Res* 2014;**74**:2688–97
40. Rodner E, Bocklitz T, von Eggeling F, Ernst G, Chernavskaia O, Popp J, Denzler J, Guntinas-Lichius O. Fully convolutional networks in multimodal nonlinear microscopy images for automated detection of head and neck carcinoma: pilot study. *Head Neck* 2019;**41**:116–21
41. Li L-H, Chen Z-F, Wang X-F, Liu X, Jiang W-Z, Zhuo S-M, Jiang L-W, Guan G-X, Chen J-X. Monitoring neoadjuvant therapy responses in rectal cancer using multimodal nonlinear optical microscopy. *Oncotarget* 2017;**8**:107323–33
42. Chu S-W, Tai S-P, Liu T-M, Sun C-K, Lin C-H. Selective imaging in second-harmonic-generation microscopy with anisotropic radiation. *J Biomed Opt* 2009;**14**:010504
43. Légaré F, Pfeffer C, Olsen BR. The role of backscattering in SHG tissue imaging. *Biophys J* 2007;**93**:1312–20
44. Chen X, Raggio C, Campagnola PJ. Second-harmonic generation circular dichroism studies of osteogenesis imperfecta. *Opt Lett* 2012;**37**:3837–9
45. Tiaho F, Recher G, Rouède D. Estimation of helical angles of myosin and collagen by second harmonic generation imaging microscopy. *Opt Exp* 2007;**15**:12286–95
46. Chu S-W, Chen S-Y, Chern G-W, Tsai T-H, Chen Y-C, Lin B-L, Sun C-K. Studies of $\chi((2))/\chi((3))$ tensors in Submicron-Scaled Bio-Tissues by polarization harmonics optical microscopy. *Biophys J* 2004;**86**:3914–22
47. Zhuo Z-Y, Liao C-S, Huang C-H, Yu J-Y, Tzeng Y-Y, Lo W, Dong C-Y, Chui H-C, Huang Y-C, Lai H-M, Chu S-W. Second harmonic generation imaging – a new method for unraveling molecular information of starch. *J Struct Biol* 2010;**171**:88–94
48. Latour G, Gusachenko I, Kowalczuk L, Lamarre I, Schanne-Klein MC. In vivo structural imaging of the cornea by polarization-resolved second harmonic microscopy. *Biomed Opt Exp* 2012;**3**:1–15
49. Chen W-L, Li T-H, Su P-J, Chou C-K, Fwu PT, Lin S-J, Kim D, So PTC, Dong C-Y. Second harmonic generation χ tensor microscopy for tissue imaging. *Appl Phys Lett* 2009;**94**:183902
50. Erikson A, Ortegren J, Hompland T, CdL D, Lindgren M. Quantification of the second-order nonlinear susceptibility of collagen I using a laser scanning microscope. *J Biomed Opt* 2007;**12**:044002
51. Williams RM, Zipfel WR, Webb WW. Interpreting Second-Harmonic generation images of collagen I fibrils. *Biophys J* 2005;**88**:1377–86

(Received April 6, 2020, Accepted May 22, 2020)